# Rossby Wave Analysis of Subsurface Temperature Fluctuations along the Honolulu–San Francisco Great Circle

JAMES MICHAEL PRICE

*Institut für Meereskunde an der Universität Kiel, Kiel, West Germany*

LORENZ MAGAARD

*Department of Oceanography, University of Hawaii, Honolulu 96822*

(Manuscript received 21 May 1982, in final form 8 October 1982)

ABSTRACT

Seven years of XBT observations collected between Honolulu and San Francisco reveal subsurface temperature fluctuations with strong, in-phase vertical coherence and fair horizontal coherence over 1000 km distances. Their annual and semi-annual harmonics exhibit randomness of phase, suggesting that the fluctuations are modeled better as a stochastic process than as a deterministic signal.

Cross-spectral fitting of a stochastic, first baroclinic mode Rossby wave model to the fluctuations demonstrates that Rossby waves could be producing 50–60% of the observed subsurface covariance at periods exceeding nine months. Phase is seen to propagate northwestward and energy westward and southwestward. The corresponding sea surface velocities and sea level fluctuations are of the order 1 cm $s^{-1}$ and 1.5 cm.

## 1. Introduction

Studies of baroclinic Rossby waves based on observations have been possible only recently, through the compilation of hydrographic data of sufficient spatial and temporal coverage. Emery and Magaard (1976) and Magaard and Price (1977) analyzed time sequences of expendable bathythermograph (XBT) observations between Hawaii and weather station November (30°N, 140°W). Price and Magaard (1980) analyzed time sequences of baroclinic potential energy in the central North Pacific, and Kang and Magaard (1980) availed themselves of the TRANSPAC XBT data collected under the NORPAX project.

In this study, we employ the unusually good XBT coverage along the great circle route between Honolulu and San Francisco. This section contains the area studied by Emery and Magaard (1976) and Magaard and Price (1977) and thereby constitutes an extension of their work. In addition, the section transects the California current, and thus a knowledge of the possible shear modes in the current is required.

The first baroclinic shear mode in the California current has been numerically determined by Kang, *et al.*, (1982), using a potential density and mean geostrophic current climatology. We incorporate the shear mode and its accompanying eigenvalues in a simple stochastic wave model and least squares fit model cross-spectra to cross-spectra of time sequences of temperature in the California current.

In addition, we fit model cross-spectra to cross-spectra of time sequences of temperature in a region where the mean background current will be neglected (Oahu to station November, 30°N, 140°W).

The consistency of our model is preliminarily checked against the dominant space- and time-scales of the data.

After we had finished preparation of this manuscript a new paper by White and Saur (1981) appeared. That paper deals with an extended version of the XBT data set used in this study. It uses a different approach and is restricted to fluctuations of annual period, while our paper deals with the period range from the cut-off period of first mode baroclinic Rossby waves (6–9 months) to 42.5 months. A comparison between the papers is given in the Appendix.

## 2. The data and preliminary analysis

Expendable bathythermograph observations were made from commercial ships sailing between Honolulu and San Francisco in a program directed by the National Marine Fisheries Service. The observations made from June 1966 through December 1974 were compiled into a long-term, seasonally varying, mean temperature field (Saur *et al.*, 1979). Dorman and Saur (1978) calculated the temperature anomalies about this mean field and mapped them onto a 92 km partition of the great circle section between Oahu and the Farallon Islands, off San Francisco, at selected depths and at 15-day intervals.

We combined the long-term mean field and the

mapped anomalies to obtain temperature–time sequences at each grid point in the section. A small number of temperature inversions below 90 m were eliminated by linearly interpolating in the vertical coordinate, and most of the first two years of data were excluded since they lacked observations down to 500 m. The resultant field was smoothed in time with a running-mean averaging with weights (0.25, 0.50, 0.25) and re-digitized at 30-day intervals (for computational economy).

As a preliminary survey of the field, each of the 15-day sections were contoured and photographed in sequence on movie film to create an animation of isotherm displacements. Viewing the film in slow motion, one can see what appears to us as random episodes of wave-like disturbances below 200 m. These disturbances propagate over a distance of one or two wavelengths (seen to be about 1000 km long), rapidly attenuating to extinction, all within roughly 6–12 months. The direction of phase propagation is seen to be usually southwestward, but northeastward propagation is also seen. In addition, strong first mode behavior in the vertical displacement of the isotherms below 200 m is seen, wherein they move up and down predominantly in phase with each other.

The movie seems to substantiate two assumptions explicit in the wave model used in this and earlier studies to model the subsurface temperature (density) fluctuations: the randomness of phase and the predominance of a vertically standing first mode. A quantitative demonstration of these features is now presented.

To establish a measure of the randomness of phase, the following procedure was undertaken. The temperature-time sequences at each grid point were partitioned into seven consecutive 12-month segments. A 12-month sinusoid was then fitted by least-squares to each segment, after subtracting the mean temperature, with amplitude and phase as free parameters. The standard deviation of the seven phases is taken as the measure of the randomness of phase in the annual signal at that grid point. Similarly, partitioning each temperature–time sequence into 14 consecutive 6-month segments and determining the standard deviation of the phases of the 6-month harmonic yields a measure of randomness in the semi-annual signal.

The 12- and 6-month harmonics were chosen because they are high energy components of the Fourier decomposition of the temperature sequences.

Most of the standard deviations of phase below 150 m in the 12-month case (Fig. 1) are of the order of 100°. [An equally distributed phase over the interval (−180°, +180°) results in a standard deviation of 104°.] The phase appears to be random below the mixed layer. In contrast, the surface layer exhibits only small variance in phase, reflecting the persistence of the strong seasonal heating and cooling at these latitudes.

There appears to be no horizontal pattern to Fig. 1. Phase is as random near the continent as it is near Hawaii.

In the 6-month case (Fig. 2), there appears to be no pattern horizontally or vertically. The standard deviation is roughly 100° everywhere, even in the surface layer.

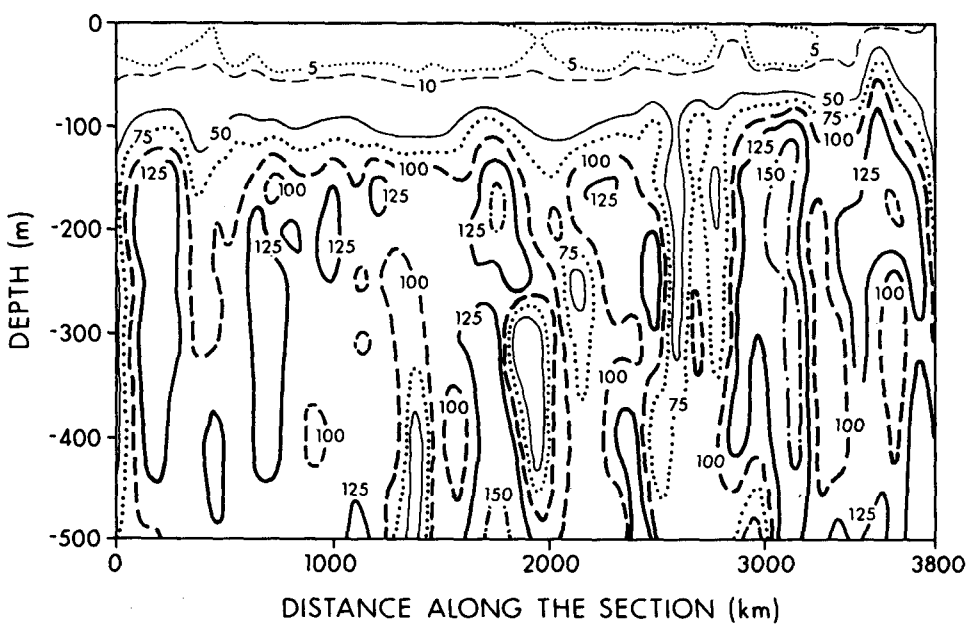


FIG. 1. Standard deviation of phase of the annual harmonic of temperature fluctuations in the Oahu–Farallon section. Contours are labeled in angular degrees.

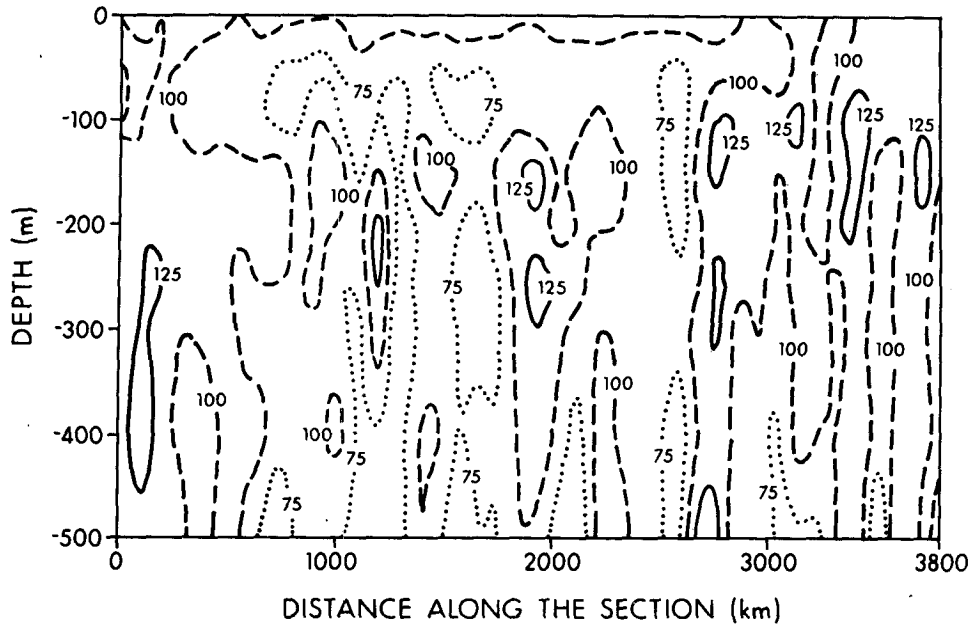


FIG. 2. As in Fig. 1 except for the semiannual harmonic.

To investigate the apparent vertical coherence seen in the movie, various cross-spectra were computed. At a location 2500 km from Oahu (roughly mid-section) the cross–spectrum between temperature at 250 m and at 400 m (Fig. 3A) shows high coherence and nearly zero phase at almost all frequencies. The cross-spectrum between temperature at 250 and 500 m (Fig. 3B) shows high coherence and nearly zero phase at several frequencies. These spectra are typical of several examined and demonstrate that the assumption of the predominance of a vertically standing first mode is reasonable.

Fairly high coherence is also seen horizontally over 1000 km distances. The cross–spectrum between temperature at 500 m depth, 1200 km from Oahu and temperature at the same depth, 2500 km from Oahu (Fig. 3C) reveals significant coherence at several frequencies (not including the annual). The cross–spectrum between temperature at 500 m, 2500 km from Oahu and temperature at 500 m, 3400 km from Oahu (Fig. 3D) also shows significant coherence at several frequencies (including the annual).

Thus, a baroclinic Rossby wave model is consistent with some of the more prominent space- and time-scales manifest in the data.

## 3. The method of analysis

The authors apply an inverse method (a cross-spectral fit) that is essentially the same as that used by Kang and Magaard (1980), henceforth referred to as KM. We attribute the subsurface (250–500 m) temperature fluctuations to a superposition of uncorrelated, first baroclinic mode Rossby waves, derive a model cross-spectrum function with wavenumber and energy as free parameters, and least squares fit the function to cross-spectra of the temperature fluctuations. The details of the method as well as the nomenclature will not be repeated; only the differences from the KM study will be discussed here.

In this study, the data grid is horizontally co-linear, and thus only a wavenumber component along the section can be resolved. (The trans-section wavenumber component is inferred from a dispersion relation.) Thus, instead of the three free model parameters used by KM, we have only two: a long section wavenumber $\kappa$ and energy density $\epsilon(\omega)$.

The standing vertical mode structure $\tilde{T}_1(\kappa,z)$ is determined for two current regimes: a region in the interior of the subtropical gyre, wherein the mean currents are neglected, and the California current, which, unlike the North Pacific drift studied by KM, is not wholly zonal (or meridional). The first region, region I, is that part of the section between Oahu and weather station N (30°N, 140°W). The dynamic topography (0/500 db) of this region, computed from these temperature data, predominantly shows weak, southerly flow (Price, 1981). The second region, region II, extends from the weather station to the continental shelf, transecting (among other things) the comparatively strong California current. Fig. 4 indicates the locations at which Väisälä frequency representing region I, and Väisälä frequency and geostrophic current representing region II were computed from a long term climatological mean density field derived from the National Oceanographic Data Center's hydrographic archive. The region II profiles are shown in Fig. 5.

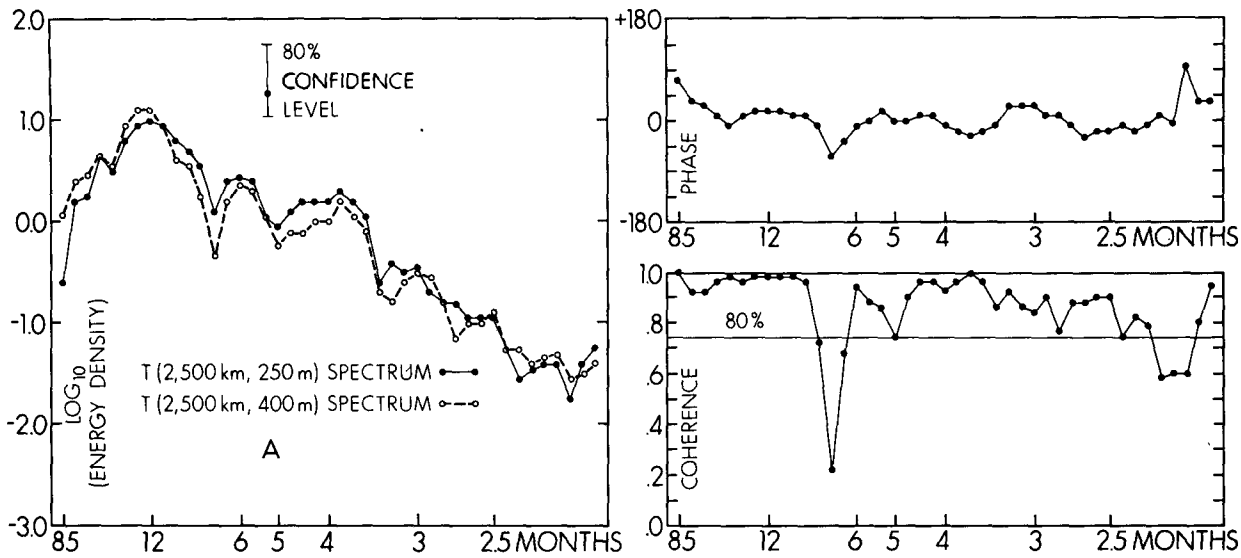


FIG. 3A. Autospectra of, and coherence and phase between temperature at 250 m and 400 m at 2500 km from Oahu.

The more general case of mesoscale plane waves in a current with a non-negligible meridional component, and with continuous stratification was studied by Kang, *et al.* (1982). In this more general derivation, the amplitude of the wave-induced pressure fluctuations $p$ is the solution of

$$(\kappa U + \eta V - \omega)\left[\frac{d}{dz}\left(\frac{f^2}{N^2}\frac{d\tilde{p}}{dz}\right) - \kappa^2\tilde{p}\right] + \left[\kappa\beta - \kappa\frac{\partial}{\partial z}\left(\frac{f^2}{N^2}\frac{\partial U}{\partial z}\right) - \eta\frac{\partial}{\partial z}\left(\frac{f^2}{N^2}\frac{\partial V}{\partial z}\right)\right]\tilde{p} = 0, \quad (3.1)$$

with boundary conditions

$$(\kappa U + \eta V - \omega)\frac{d\tilde{p}}{dz} - \left(\kappa\frac{\partial U}{\partial z} + \eta\frac{\partial V}{\partial z}\right)\tilde{p} = 0 \quad \text{at } z = 0 \text{ and at } z = -H, \quad (3.2)$$

where

| | |
|---|---|
| $(\kappa, \eta)$ | wavenumber vector |
| $(U, V)$ | mean current velocity |
| $\omega$ | angular wave frequency |
| $N$ | Brunt–Väisälä frequency |
| $f$ | Coriolis parameter |
| $(x, y, z)$ | Cartesian coordinates measured eastward, northward, and upward, respectively |

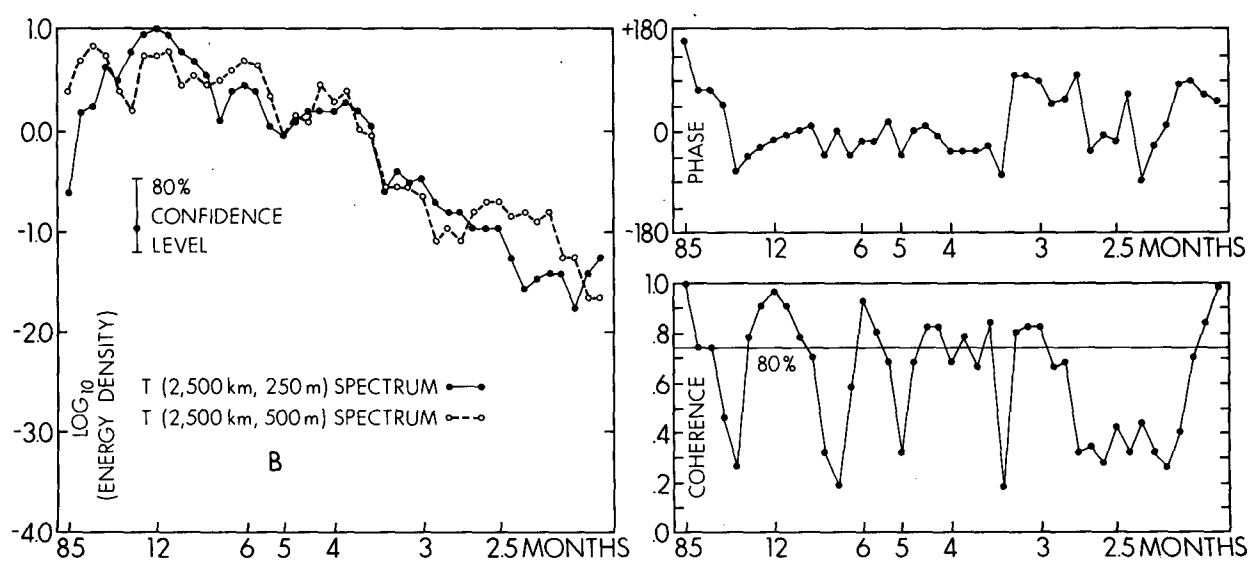


FIG. 3B. Autospectra of, and coherence and phase between temperature at 250 m and 500 m at 2500 km from Oahu.

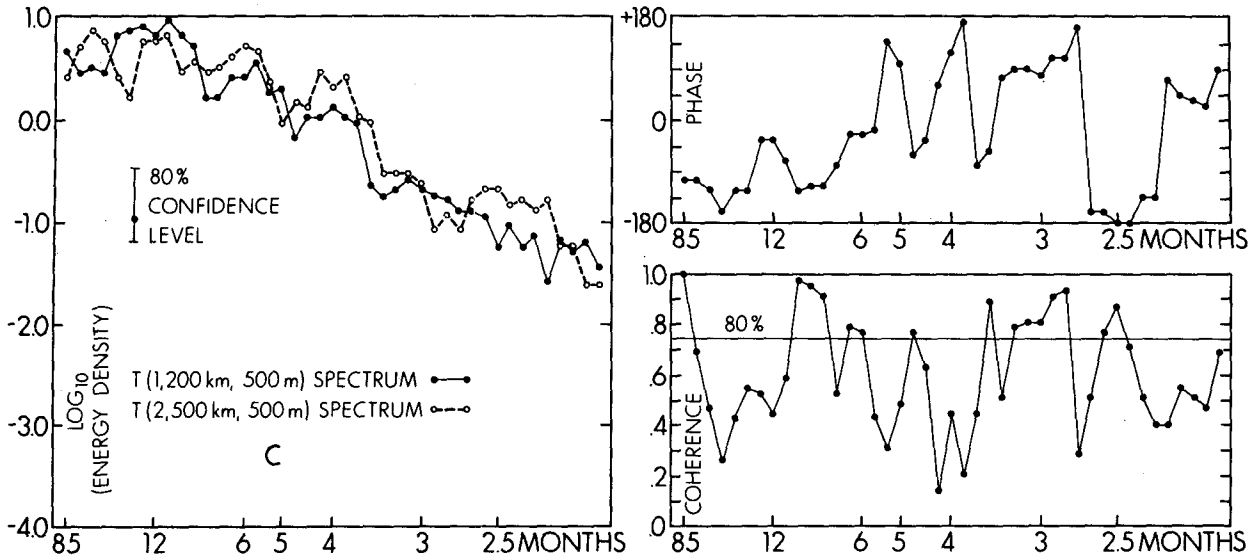


FIG. 3C. Autospectra of, and coherence and phase between temperature horizontally separated by 1300 km, at 500 m depth, in the central portion of the Oahu–Farallon section.

$\beta$ meridional gradient of $f$
$H$ depth of the ocean bottom.

Numerical solutions were obtained for region I using the representative $N^2$-profile, assuming a flat bottom and ignoring mean $U$ and $V$, and for region II using the representative $N^2$-, $U$-, and $V$-profiles and assuming a flat bottom. Three examples of first mode eigenfunctions in region II are shown in Fig. 6.

The eigenfunctions are seen to only weakly depend upon wavelength in the range 500 to 5000 km, and, as a simplifying assumption, this dependence is ignored (as was done by KM).

Knowledge of $\tilde{p}(z)$ yields the amplitudes of the associated wave induced velocity and temperature fluctuations:

$$\tilde{U}(z) = \frac{-i\eta}{f\rho_0}\tilde{p}(z), \tag{3.3}$$

$$\tilde{V}(z) = \frac{i\kappa}{f\rho_0}\tilde{p}(z), \tag{3.4}$$

$$\Theta_1(\omega)\tilde{T}_1(z) = \frac{1}{\rho_0\alpha g}\frac{d\tilde{p}(z)}{dz}, \tag{3.5}$$

where $\rho_0$ is a reference density, $\alpha$ the thermal expansion coefficient ($\approx 2 \times 10^{-4}$ °C$^{-1}$), $g$ the gravitational

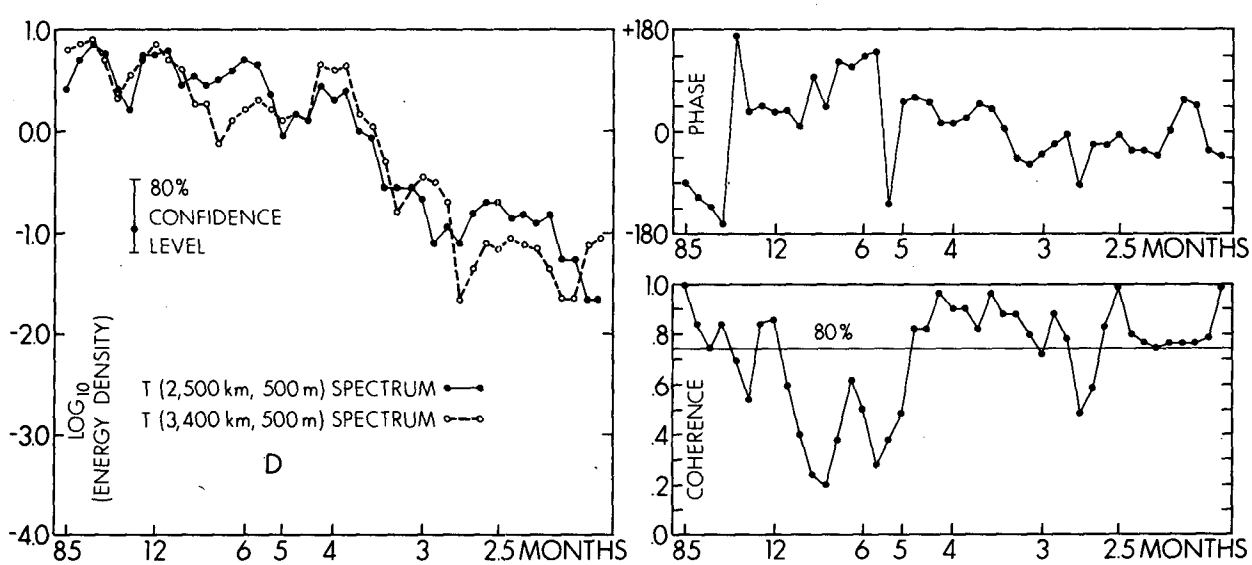


FIG. 3D. Autospectra of, and coherence and phase between temperature horizontally separated by 900 km, at 500 m depth, in the eastern portion of the Oahu–Farallon section.

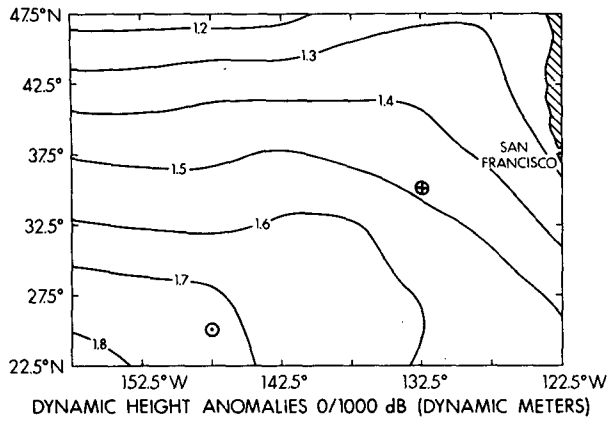


FIG. 4. Contoured dynamic height anomalies 0/1000 db (in dynamic meters) derived from a mean density field. The circled dot denotes the location where region I pressure eigensolutions were computed; the circled plus sign denotes the location where Region II pressure eigensolutions were computed.

acceleration, and the wavenumber dependence of $\Theta_1 \tilde{T}_1$ is eliminated along with that of $\tilde{p}$. The $\tilde{T}_1$-profiles representing regions I and II are shown in Fig. 7.

The associated eigenvalues yield a set of $(\kappa, \eta, \omega)$ triplets, the numerical dispersion relation of first mode baroclinic Rossby waves. The $\omega$-contours (slowness curves) of the dispersion relation applicable to region II, the California current (Fig. 8), differ considerably from those of region I with negligible mean current (Fig. 9). The former is highly asymmetric and exhibits areas wherein no solutions are found (the upper, and lower-right portions of Fig. 8). In the California current a relative maximum in frequency of $2.55 \times 10^{-7}\ s^{-1}$ (9.52 months) is found at $(\kappa, \eta) = (-2.00 \times 10^{-5}, -1.25 \times 10^{-6})\ m^{-1}$, compared to the high-frequency cut-off of $3.35 \times 10^{-7}\ s^{-1}$ (7.12 months) at $(\kappa, \eta) = (-2.80 \times 10^{-5}, 0.00)\ m^{-1}$ in the case of negligible mean current. In addition, Kang, *et al.* (1982) found solutions to (3.1) and (3.2) in the eastern half-plane in a simple two-level model. A brief (but expensive) search for numerical eastern half-plane solutions proved futile, but was not at all exhaustive; there may well be solutions for positive values of $\kappa$.

The cross-spectral fit is applied to small, non-overlapping segments of the section, positions over which the assumptions of horizontal homogeneity and unidirectionality of the wave field may be assumed. Six horizontal (by four vertical) grid points are taken at a time, thus partitioning the section into eight contiguous segments (four per region).

## 4. Results of the analysis

For each "best-fit" long section wavenumber $\kappa$ [one that minimizes $F$ in Equation (7) of KM], there may be one or two first mode baroclinic Rossby wave (FMBRW) wavenumber vectors whose orthogonal projection onto the section is $\kappa$ or is within one standard error ($\delta\kappa$) of $\kappa$. Most of the best-fit wavenumbers in the 9.4–42.5 month period range found in region I could be such projections. Their corresponding wavenumber vectors of both long and short wavelengths point northwestward. The group velocities corresponding to the long wavelengths point westward; those of the short wavelengths, southwestward.

The 14- and 28-month cases in region I are in fair agreement with the findings of Emery and Magaard (1976).

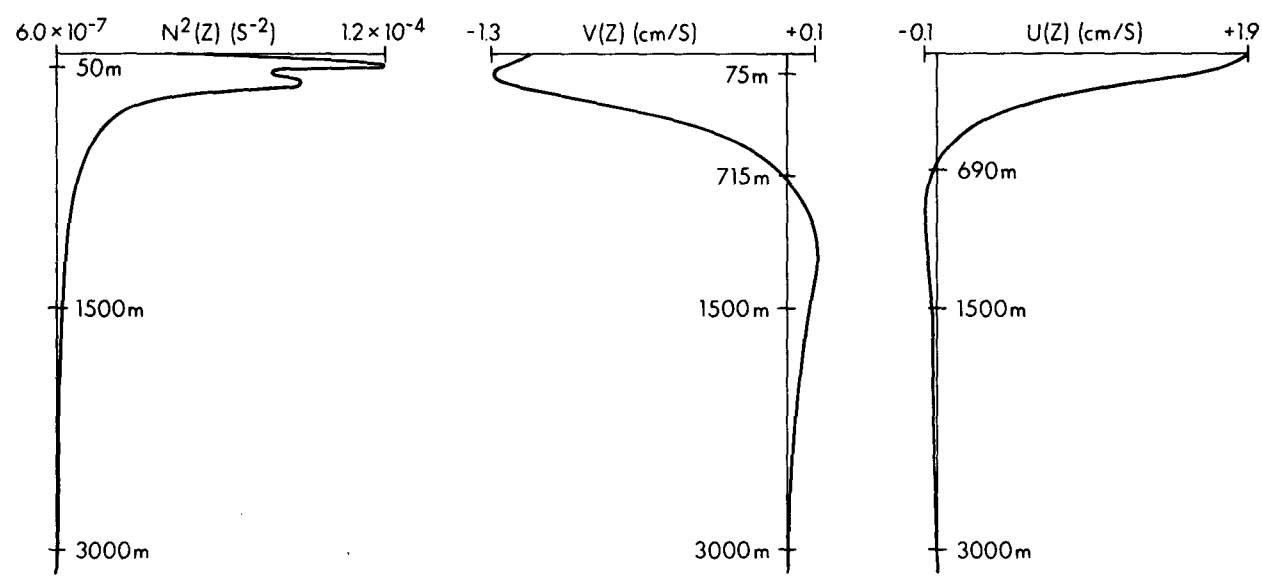


FIG. 5. Brunt-Väisälä frequency squared $N^2$ and meridional and zonal current speeds $V$ and $U$, derived from the mean density field in the California current. (after Kang *et al.*, 1982).

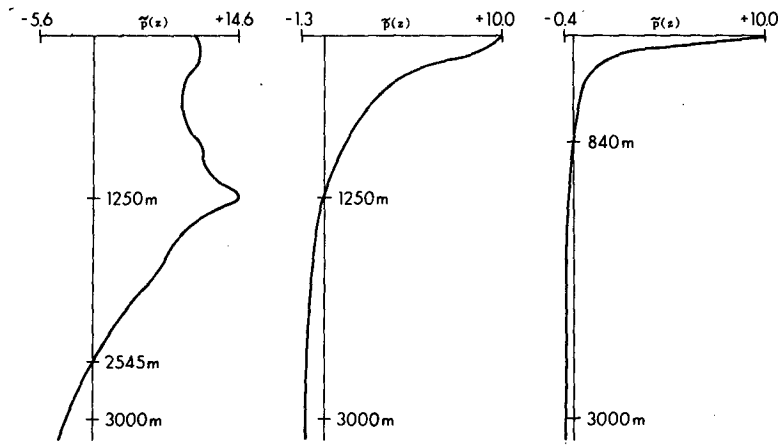


FIG. 6. Sample of first mode eigensolutions of (3.1) and (3.2). Wavelength = 200 km (left); 1000 km (center); and 5000 km (right). Values of $\tilde{p}(z)$ shown are arbitrary amplitudes.

Few of the best-fit wavenumbers in the 8.5-month and shorter period range in region I, however, could be such projections. Apparently, either FMBRW energy in this band is too low to resolve (or is zero), or the (neglected) currents in region I lengthen the cutoff period.

Using the numerically determined slowness curves, we find most of the best-fit long section wavenumbers in the 17.0–42.5 month band in region II could be those of FMBRWs. Phase propagates northwestward and energy propagates southwestward for both the long and short wavelengths. At periods shorter than 17.0 months, however, none of the best-fit wavenumbers could be those of FMBRWs (to within one and often two standard errors about $\kappa$).

It should be noted that most of the best-fit wavenumbers in the 17.0–42.5 month band in region II could also be the projections of wavenumber vectors along slowness curves computed from the region II mean density field and values of $f$ and $\beta$ but neglecting the mean current shear. (Furthermore, a few of the region II best-fit wavenumbers at shorter periods could also be projections of such FMBRWs.) The explanation for this is that for longer period, long wavelength waves with phase propagating in the direction range southwestward to north-northwestward, there is not too much difference between the two dispersion relations. Coincidently, the longer period best-fit waves fall into this category. The best-fit wavenumbers were, however, generally closer to the numerically determined slowness curves.

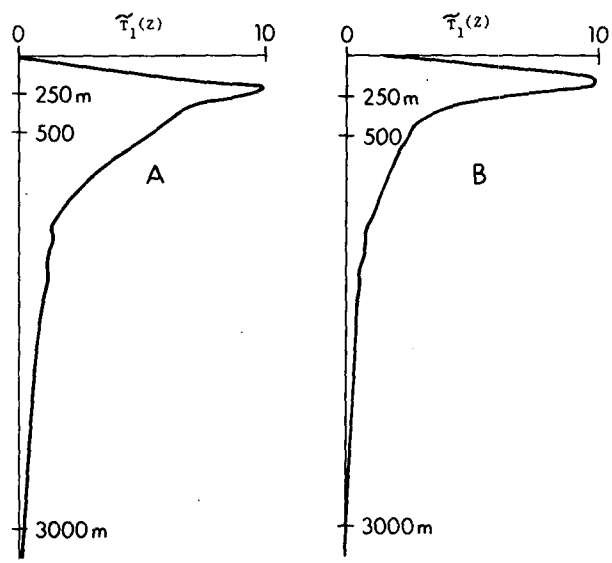


FIG. 7. First baroclinic temperature shear mode representing region I (A) and region II (B) in arbitrary, dimensionless units.

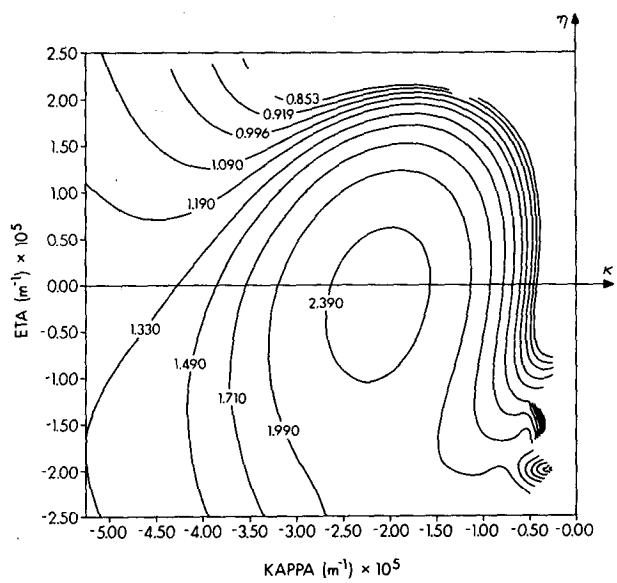


FIG. 8. Numerical slowness curves of first mode baroclinic Rossby waves in the California current (region II). Frequency contours are labeled in units of $10^{-7}$ $s^{-1}$. (after Kang *et al.*, 1982).

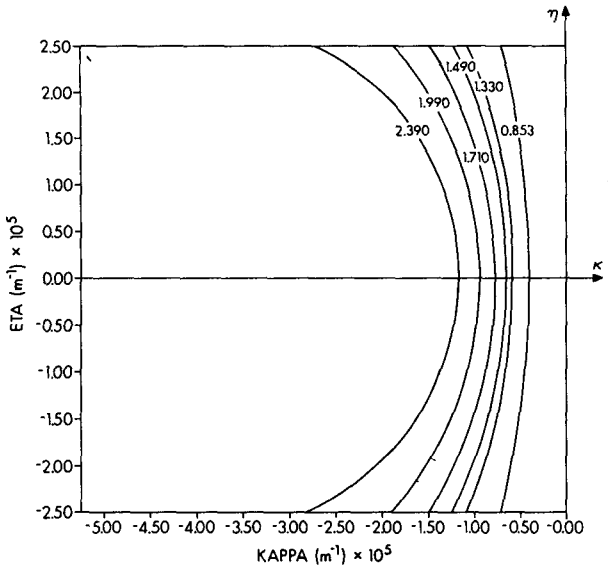


FIG. 9. Slowness curves of first baroclinic Rossby waves in a region of negligible mean current shear (region I). Frequency contours are labeled in units of $10^{-7}$ $s^{-1}$.

The wavelengths and directions of phase propagation of the inferred FMBRWs are illustrated in Figs. 10a–d for the longer wavelength waves at selected periods. Wavelengths $\gamma$, phase speeds $c$, group speeds $c_g$, and goodness-of-fit parameters $F_{min}/F_0$ (0% for a perfect fit; 100% for no fit at all) for both the long and short wavelength FMBRWs at the same periods are listed in Tables 1a–d. Angles $\gamma$ and $\phi$ (Fig. 11) indicate the directions of the wavenumber and group velocity vectors respectively and one standard error in each tabulated parameter is indicated by the prefix $\delta$. A blank entry implies that no best-fit wave was found.

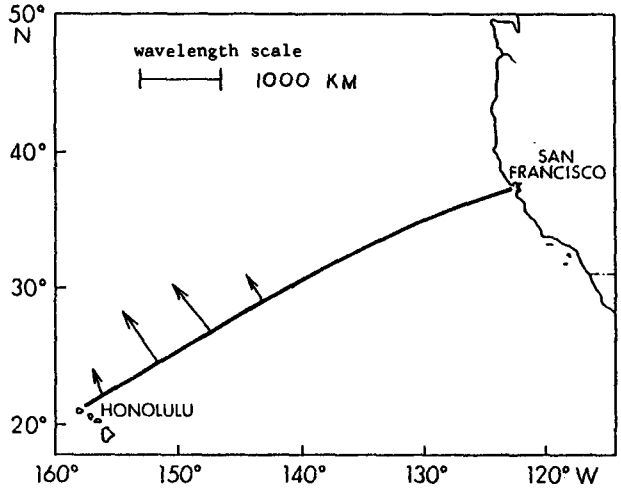


FIG. 10A. Directions of phase propagation and wavelengths (lengths of arrows) of the longer wavelength, 12.1-month period FMBRWs.

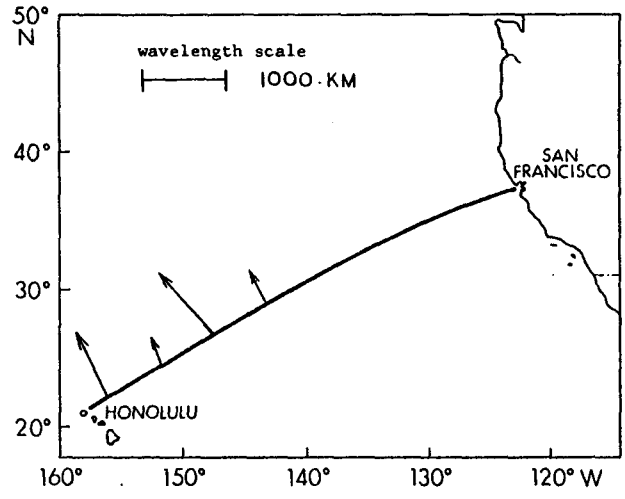


FIG. 10B. As in Fig. 10A except for 14.2-month period FMBRWs.

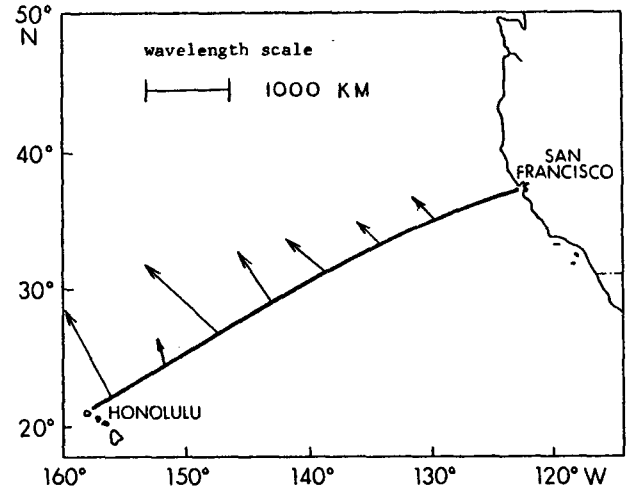


FIG. 10C. As in Fig. 10A except for 17.0-month period FMBRWs.

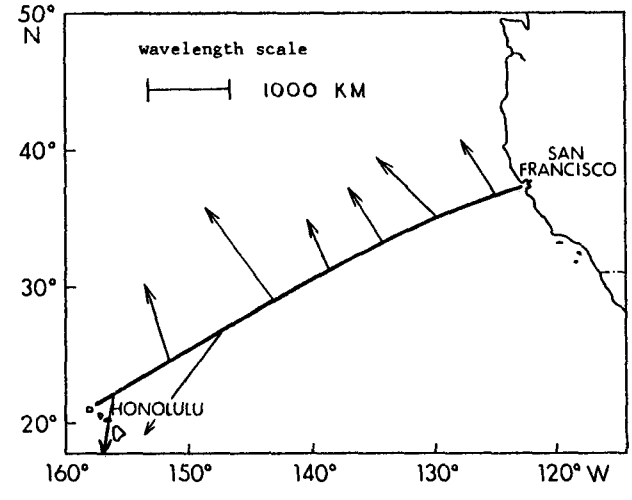


FIG. 10D. As in Fig. 10A except for 28.3-month period FMBRWs.

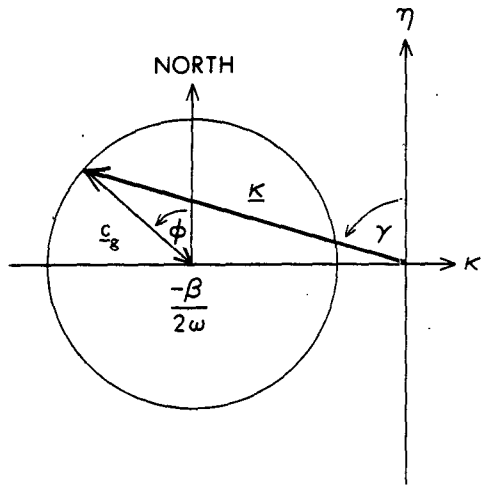


FIG. 11. Orientation of the best-fit wavenumber vector $\kappa$ and best-fit group velocity vector $C_g$. Angles $\gamma$ and $\phi$ are measured counterclockwise from geographic north. The circle is a region I slowness curve with frequency $\omega$.

Overall, we find that 50–60% of the spectrally decomposed covariance of the temperature field in the 9.4- to 42.5-month period range can be explained by FMBRWs. Their apparent amplitudes are large enough to produce sea level fluctuations of 1.5 cm and horizontal sea surface particle speeds of 1 cm $s^{-1}$ (resulting in a 100 km horizontal excursion, for example, of a surface particle displaced by a 12-month FMBRW), in good agreement with the values found by KM in the southeastern-most corner of their data field (the overlapping region between this study and theirs).

## 5. Discussion

The subsurface temperature fluctuations between Honolulu and San Francisco seem to be modeled better as a stochastic process than as a deterministic signal.

The geometry of the data grid prevents us from uniquely determining the wavenumber vectors of the

TABLE 1. Wave parameters for the 12.1-month FMBRWs.

*a. 12.1 months*

| Latitude (°N) | Longitude (°W) | Wavelength | | Wave-number direction | | Phase speed | | Group velocity direction | | Group speed | | Good-ness-of-fit | Spectral energy density | |
|---|---|---|---|---|---|---|---|---|---|---|---|---|---|---|
| (deg) | | λ (km) | δλ* | γ (deg) | δγ* | $C$ (cm $s^{-1}$) | δC* | φ (deg) | δφ* | $C_g$ (cm $s^{-1}$) | $\delta C_g^*$ | $F_{min}/F_0$ (%) | $E$ ($10^3$ °C² month) | δE* |
| 22.4 | 155.9 | 323. | 185. | 21. | 1. | 1.02 | 0.58 | −68.0 | 13.5 | 2.70 | 1.62 | 65. | 2.81 | 1.15 |
| 22.4 | 155.9 | 140. | 36. | 30. | 6. | 0.44 | 0.11 | −38.6 | 13.5 | 0.84 | 0.37 | 65. | | |
| 24.8 | 152.2 | 755. | 575. | 34. | 22. | 2.37 | 1.81 | −81.3 | 8.6 | 3.84 | 0.89 | 59. | 2.57 | 0.91 |
| 24.8 | 152.2 | 120. | 15. | 35. | 4. | 0.38 | 0.05 | −28.1 | 8.6 | 0.61 | 0.13 | 59. | | |
| 27.1 | 148.3 | 709. | 278. | 39. | 13. | 2.23 | 0.87 | −81.3 | 5.0 | 3.19 | 0.35 | 21. | 3.56 | 0.67 |
| 27.1 | 148.3 | 130. | 10. | 35. | 2. | 0.41 | 0.03 | −31.2 | 5.0 | 0.65 | 0.08 | 21. | | |
| 29.3 | 144.3 | 382. | 186. | 31. | 6. | 1.20 | 0.59 | −71.0 | 11.1 | 2.06 | 0.67 | 28. | 2.75 | 0.73 |
| 29.3 | 144.3 | 172. | 41. | 31. | 3. | 0.54 | 0.13 | −45.2 | 11.1 | 0.92 | 0.30 | 28. | | |
| 31.4 | 140.1 | | | | | | | | | | | | | |
| 31.4 | 140.1 | | | | | | | | | | | | | |
| 33.3 | 135.7 | | | | | | | | | | | | | |
| 33.3 | 135.7 | | | | | | | | | | | | | |
| 35.1 | 131.2 | | | | | | | | | | | | | |
| 35.1 | 131.2 | | | | | | | | | | | | | |
| 36.7 | 126.4 | | | | | | | | | | | | | |
| 36.7 | 126.4 | | | | | | | | | | | | | |

*b. 14.2 months*

| | | | | | | | | | | | | | | |
|---|---|---|---|---|---|---|---|---|---|---|---|---|---|---|
| 22.4 | 155.9 | 864. | 695. | 26. | 17. | 2.31 | 1.86 | −83.3 | 6.0 | 4.96 | 1.10 | 56. | 3.18 | 1.09 |
| 22.4 | 155.9 | 93. | 7. | 35. | 3. | 0.25 | 0.02 | −23.3 | 6.0 | 0.41 | 0.06 | 56. | | |
| 24.8 | 152.2 | 347. | 226. | 20. | 2. | 0.93 | 0.61 | −72.1 | 12.3 | 2.56 | 1.47 | 62. | 2.54 | 0.99 |
| 24.8 | 152.2 | 119. | 26. | 30. | 5. | 0.32 | 0.07 | −37.3 | 12.3 | 0.61 | 0.24 | 62. | | |
| 27.1 | 148.3 | 960. | 478. | 43. | 23. | 2.57 | 1.28 | −85.0 | 4.4 | 3.50 | 0.29 | 25. | 3.20 | 0.71 |
| 27.1 | 148.3 | 104. | 7. | 35. | 2. | 0.28 | 0.02 | −27.6 | 4.4 | 0.46 | 0.05 | 25. | | |

TABLE 1. (*Continued*)

*b. 14.2 months*

| Latitude (°N) | Longitude (°W) | Wavelength | | Wave-number direction | | Phase speed | | Group velocity direction | | Group speed | | Good-ness-of-fit | Spectral energy density | |
|---|---|---|---|---|---|---|---|---|---|---|---|---|---|---|
| | | $\lambda$ | $\delta\lambda$* | $\gamma$ | $\delta\gamma$* | $C$ | $\delta C$* | $\phi$ | $\delta\phi$* | $C_g$ | $\delta C_g$* | $F_{min}/F_0$ | $E$ | $\delta E$* |
| (deg) | | (km) | | (deg) | | (cm s$^{-1}$) | | (deg) | | (cm s$^{-1}$) | | (%) | ($10^3$ °C$^2$ month) | |
| 29.3 | 144.3 | 464. | 239. | 28. | 8. | 1.24 | 0.64 | −76.9 | 7.8 | 2.39 | 0.61 | 27. | 3.28 | 0.84 |
| 29.3 | 144.3 | 129. | 19. | 31. | 3. | 0.35 | 0.05 | −39.3 | 7.8 | 0.62 | 0.14 | 27. | | |
| 31.4 | 140.1 | | | | | | | | | | | | | |
| 31.4 | 140.1 | | | | | | | | | | | | | |
| 33.3 | 135.7 | | | | | | | | | | | | | |
| 33.3 | 135.7 | | | | | | | | | | | | | |
| 35.1 | 131.2 | | | | | | | | | | | | | |
| 35.1 | 131.2 | | | | | | | | | | | | | |
| 36.7 | 126.4 | | | | | | | | | | | | | |
| 36.7 | 126.4 | | | | | | | | | | | | | |

*c. 17.0 months*

| | | | | | | | | | | | | | | |
|---|---|---|---|---|---|---|---|---|---|---|---|---|---|---|
| 22.4 | 155.9 | 1217. | 1048. | 29. | 24. | 2.72 | 2.34 | −86.1 | 3.9 | 5.42 | 0.72 | 43. | 3.12 | 0.92 |
| 22.4 | 155.9 | 74. | 4. | 36. | 2. | 0.17 | 0.01 | −20.4 | 3.9 | 0.27 | 0.03 | 43. | | |
| 24.8 | 152.2 | 355. | 179. | 16. | 1. | 0.79 | 0.40 | −75.8 | 7.3 | 2.69 | 1.15 | 53. | 2.57 | 0.90 |
| 24.8 | 152.2 | 92. | 11. | 30. | 3. | 0.21 | 0.02 | −33.6 | 7.3 | 0.39 | 0.09 | 53. | | |
| 27.1 | 148.3 | 1225. | 961. | 47. | 47. | 2.74 | 2.15 | −86.7 | 5.2 | 3.68 | 0.36 | 48. | 1.64 | 0.56 |
| 27.1 | 148.3 | 84. | 6. | 34. | 2. | 0.19 | 0.01 | −25.8 | 5.2 | 0.32 | 0.04 | 48. | | |
| 29.3 | 144.3 | 716. | 534. | 32. | 20. | 1.60 | 1.20 | −83.2 | 6.4 | 2.85 | 0.54 | 56. | 1.18 | 0.40 |
| 29.3 | 144.3 | 95. | 10. | 32. | 3. | 0.21 | 0.02 | −33.0 | 6.4 | 0.38 | 0.07 | 56. | | |
| 31.4 | 140.1 | 657. | 428. | 49. | 14. | 1.47 | 1.31 | −86.2 | 3.6 | 1.50 | 0.22 | 83. | 0.47 | 0.36 |
| 33.3 | 135.7 | 419. | 307. | 45. | 20. | 0.94 | 0.72 | −65.8 | 2.6 | 1.24 | 0.35 | 28. | 1.79 | 0.41 |
| 35.1 | 131.2 | 388. | 256. | 45. | 16. | 0.87 | 0.66 | −60.4 | 4.2 | 1.14 | 0.26 | 52. | 1.18 | 0.45 |
| 36.7 | 126.4 | | | | | | | | | | | | | |

*d. 28.3 months*

| | | | | | | | | | | | | | | |
|---|---|---|---|---|---|---|---|---|---|---|---|---|---|---|
| 22.4 | 155.9 | 732. | 645. | 169. | 7. | 0.98 | 0.87 | −94.2 | 3.4 | 4.84 | 1.46 | 73. | 1.50 | 0.79 |
| 22.4 | 155.9 | 40. | 1. | 39. | 2. | 0.05 | 0.00 | −12.4 | 3.4 | 0.08 | 0.01 | 73. | | |
| 24.8 | 152.2 | 991. | 865. | 17. | 13. | 1.33 | 1.16 | −86.9 | 2.7 | 4.38 | 0.69 | 44. | 4.07 | 1.33 |
| 24.8 | 152.2 | 46. | 2. | 34. | 1. | 0.06 | 0.00 | −22.4 | 2.7 | 0.11 | 0.01 | 44. | | |
| 27.1 | 148.3 | 1603. | 2311. | 143. | 74. | 2.15 | 3.10 | −92.0 | 4.0 | 3.83 | 0.49 | 69. | 1.95 | 1.02 |
| 27.1 | 148.3 | 46. | 2. | 35. | 2. | 0.06 | 0.00 | −20.5 | 4.0 | 0.10 | 0.01 | 69. | | |
| 29.3 | 144.3 | 1445. | 1304. | 36. | 37. | 1.94 | 1.75 | −88.1 | 2.5 | 3.29 | 0.22 | 37. | 3.21 | 0.87 |
| 29.3 | 144.3 | 52. | 2. | 32. | 1. | 0.07 | 0.00 | −28.1 | 2.5 | 0.13 | 0.01 | 37. | | |
| 31.4 | 140.1 | 628. | 453. | 25. | 08. | 0.85 | 0.62 | −87.0 | 4.8 | 1.77 | 0.63 | 58. | 0.58 | 0.21 |
| 33.3 | 135.7 | 838. | 621. | 32. | 38. | 1.14 | 0.99 | −90.1 | 6.0 | 1.84 | 0.22 | 38 | 1.23 | 0.36 |
| 35.1 | 131.2 | 1122. | 1049. | 45. | 29. | 1.52 | 1.06 | −93.7 | 5.5 | 2.31 | 0.34 | 57. | 0.70 | 0.22 |
| 36.7 | 126.4 | 838. | 744. | 32. | 41. | 1.14 | 1.08 | −90.1 | 7.2 | 1.84 | 0.31 | 49. | 1.30 | 0.45 |

* Prefix $\delta$ indicates one standard error.

prevailing field. However, previous studies (Emery and Magaard, 1976; Magaard and Price, 1977; and Price and Magaard, 1980) were able to demonstrate the existence of Rossby waves in this area, and on the strength of their findings, we hypothesize the predominance of this wave type.

In the region of overlap between these earlier studies and ours, there is fair agreement among the best-fit wavenumbers. In addition, most of the best-fit wavenumbers found along the section are oriented roughly perpendicular to the section, ie. in the direction in which a linear array is most directionally sensitive. Thus it seems that the (horizontal) one-dimensionality of the data grid is not a serious liability.

By modeling the fluctuations as those produced by a field of uncorrelated first baroclinic mode Rossby waves, 50–60% of the spectrally decomposed covariance at the longer periods is explained. The failure to model fluctuations of periods shorter than 9.4 months may be due to the lengthening of the cut-off period by the local mean current.

The influence of even a comparatively weak eastern boundary current on Rossby wave dispersion is not at all negligible. Since the geostrophic flow across the section exhibits considerable temporal and spatial variance (Price, 1981), a more elaborate theory incorporating a time-varying mean current might improve the fit in the region of the California current.

*Acknowledgments.* We wish to thank C. E. Dorman and J. F. T. Saur for making the objectively analyzed XBT data available for this study. D. R. McLain's efforts in the acquisition and preliminary processing of the raw XBT data are gratefully acknowledged.

This research has been supported by the Office of Naval Research under the North Pacific Experiment of the International Decade of Ocean Exploration; this support is much appreciated. This paper is Hawaii Institute of Geophysics Contribution No. 1311.

## APPENDIX

### Comparison with an Earlier Study

White and Saur (1981) have developed a model for annual baroclinic Rossby waves emanating from a line source near the coast of California, where they are generated by large-amplitude annual fluctuations of the wind stress curl. White and Saur (1981) compare this model with observations as follows: They calculate the mean annual cycle of the displacements of the 9°C isotherm (after removing the effect of local Ekman pumping) at each standard location between Honolulu and San Francisco and fit a sine-wave to it resulting in a value for the amplitude and phase at each location. They compare these values with the corresponding model values (Fig. 8 of their paper). The comparison is not done in any quantitative way, just by inspection. Examining their Fig. 8, we could rate the agreement between their model and their observed values as good for the longitudinal range from 125 to 135°W, fair for the range from 135 to 148°W (poor agreement of amplitudes), and poor for the range from 148 to 156°W (total disagreement of phases, however good agreement of amplitudes). We would interpret this result as showing that phase coupling of the waves with the remote generating agent becomes weaker with distance from the source and disappears entirely west of about 148°W.

Contrary to White and Saur's model, our model rests on the assumption of random amplitudes and phases. Comparing our results for the annual period with theirs, we find that our model works well for the range from 144° to 156°W, whereas east of 144°W it does not work in the sense that we do not find annual Rossby waves with random phase there. This is in total agreement with the idea that the westward propagating waves loose their phase connection with the fluctuations in the source region gradually.

In the transition zone from 144° to 148°W both approaches produce similar results concerning amplitudes, wavelengths and directions of propagation. Our model does not lead to absolute phases by definition.

In view of the findings we consider the two approaches complementary.

## REFERENCES

Dorman, C. E., and J. F. T. Saur, 1978: Temperature anomalies between San Francisco and Honolulu, 1966–74, gridded by an objective analysis. *J. Phys. Oceanogr.*, **8,** 247–257.

Emery, W. J., and L. Magaard, 1976: Baroclinic Rossby waves as inferred from temperature fluctuations in the eastern Pacific. *J. Mar. Res.*, **34,** 365–385.

Kang, Y. Q., and L. Magaard, 1980: Annual baroclinic Rossby waves in the central North Pacific. *J. Phys. Oceanogr.*, **10,** 1159–1167.

——, J. M. Price and L. Magaard, 1982: On stable and unstable Rossby waves in non-zonal oceanic shear flow. *J. Phys. Oceanogr.*, **6,** 528–537.

Magaard, L., and J. M. Price, 1977: Note on the significance of a previous Rossby wave fit to internal temperature fluctuations in the eastern Pacific. *J. Mar. Res.*, **35,** 649–651.

Price, J. M., 1981: Monthly mean sea level fluctuations at Honolulu and San Francisco and the intervening geostrophic currents. *J. Phys. Oceanogr.*, **11,** 1375–1382.

——, and L. Magaard, 1980: Rossby wave analysis of the baroclinic potential energy in the upper 500 meters of the North Pacific. *J. Mar. Res.*, **38,** 249–264.

Saur, J. F. T., L. E. Eber, D. R. McLain, and C. E. Dorman, 1979: Vertical sections of semimonthly mean temperature on the San Francisco-Honolulu route: from expendable bathythermograph observations, June 1966–December 1974. NOAA Tech. Rep., NMFS SSRF-728, 35 pp.

White, W. B., and J. F. T. Saur, 1981: A source of annual baroclinic waves in the eastern subtropical North Pacific. *J. Phys. Oceanogr.*, **11,** 1452–1462.